Author(s): Adare, A.; Afanasiev, S.; Aidala, C.; Ajitanand, N. N.; Akiba, Y.; Al-Bataineh, H.; Alexander, J.; Angerami, A.; Aoki, K.; Apadula, N.; Kim, Dong Jo; Rak, Jan

Title: Heavy-flavor electron-muon correlations in p+p and d+Au collisions at sNN−−−−√=200 GeV

Year: 2014

Version:

Please cite the original version:

Adare, A., Afanasiev, S., Aidala, C., Ajitanand, N.N., Akiba, Y., Al-Bataineh, H., Alexander, J., Angerami, A., Aoki, K., Apadula, N., Kim, D. J., & Rak, J. (2014). Heavy-flavor electron-muon correlations in p+p and d+Au collisions at sNN−−−−√=200 GeV. Physical Review C, 89(3), Article 034915. https://doi.org/10.1103/PhysRevC.89.034915

Heavy-flavor electron-muon correlations in $p + p$ and $d + \mathrm{Au}$ collisions at $\sqrt{s_{NN}} = 200$ GeV

A. Adare,[14] S. Afanasiev,[31] C. Aidala,[44,45] N. N. Ajitanand,[63] Y. Akiba,[57,58] H. Al-Bataineh,[51] J. Alexander,[63] A. Angerami,[15] K. Aoki,[36,57] N. Apadula,[64] L. Aphecetche,[65] Y. Aramaki,[13,57] J. Asai,[57] E. T. Atomssa,[37] R. Averbeck,[64] T. C. Awes,[53] B. Azmoun,[8] V. Babintsev,[25] M. Bai,[7] G. Baksay,[21] L. Baksay,[21] A. Baldisseri,[17] K. N. Barish,[9] P. D. Barnes,[40,*] B. Bassalleck,[50] A. T. Basye,[1] S. Bathe,[6,9,58] S. Batsouli,[53] V. Baublis,[56] C. Baumann,[46] A. Bazilevsky,[8] S. Belikov,[8,*] R. Belmont,[69] R. Bennett,[64] A. Berdnikov,[60] Y. Berdnikov,[60] J. H. Bhom,[73] A. A. Bickley,[14] D. S. Blau,[35] J. G. Boissevain,[40] J. S. Bok,[73] H. Borel,[17] K. Boyle,[64] M. L. Brooks,[40] H. Buesching,[8] V. Bumazhnov,[25] G. Bunce,[8,58] S. Butsyk,[40] C. M. Camacho,[40] S. Campbell,[64] A. Caringi,[47] B. S. Chang,[73] W. C. Chang,[2] J.-L. Charvet,[17] C.-H. Chen,[64] S. Chernichenko,[25] C. Y. Chi,[15] M. Chiu,[8,26] I. J. Choi,[73] J. B. Choi,[11] R. K. Choudhury,[5] P. Christiansen,[42] T. Chujo,[68] P. Chung,[63] A. Churyn,[25] O. Chvala,[9] V. Cianciolo,[53] Z. Citron,[64] B. A. Cole,[15] Z. Conesa del Valle,[37] M. Connors,[64] P. Constantin,[40] M. Csanád,[19] T. Csörgő,[72] T. Dahms,[64] S. Dairaku,[36,57] I. Danchev,[69] K. Das,[22] A. Datta,[44] G. David,[8] M. K. Dayananda,[23] A. Denisov,[25] D. d'Enterria,[37] A. Deshpande,[58,64] E. J. Desmond,[8] K. V. Dharmawardane,[51] O. Dietzsch,[61] A. Dion,[29,64] M. Donadelli,[61] O. Drapier,[37] A. Drees,[64] K. A. Drees,[7] A. K. Dubey,[71] J. M. Durham,[40,64] A. Durum,[25] D. Dutta,[5] V. Dzhordzhadze,[9] L. D'Orazio,[43] S. Edwards,[22] Y. V. Efremenko,[53] F. Ellinghaus,[14] T. Engelmore,[15] A. Enokizono,[39,53] H. En'yo,[57,58] S. Esumi,[68] K. O. Eyser,[9] B. Fadem,[47] D. E. Fields,[50,58] M. Finger,[10] M. Finger, Jr.,[10] F. Fleuret,[37] S. L. Fokin,[35] Z. Fraenkel,[71,*] J. E. Frantz,[52,64] A. Franz,[8] A. D. Frawley,[22] K. Fujiwara,[57] Y. Fukao,[36,57] T. Fusayasu,[49] I. Garishvili,[66] A. Glenn,[14,39] H. Gong,[64] M. Gonin,[37] J. Gosset,[17] Y. Goto,[57,58] R. Granier de Cassagnac,[37] N. Grau,[3,15] S. V. Greene,[69] G. Grim,[40] M. Grosse Perdekamp,[26,58] T. Gunji,[13] H.-Å. Gustafsson,[42,*] A. Hadj Henni,[65] J. S. Haggerty,[8] K. I. Hahn,[20] H. Hamagaki,[13] J. Hamblen,[66] R. Han,[55] J. Hanks,[15] E. P. Hartouni,[39] K. Haruna,[24] E. Haslum,[42] R. Hayano,[13] X. He,[23] M. Heffner,[39] T. K. Hemmick,[64] T. Hester,[9] J. C. Hill,[29] M. Hohlmann,[21] W. Holzmann,[15,63] K. Homma,[24] B. Hong,[34] T. Horaguchi,[13,24,57,67] D. Hornback,[66] S. Huang,[69] T. Ichihara,[57,58] R. Ichimiya,[57] H. Iinuma,[36,57] Y. Ikeda,[68] K. Imai,[30,36,57] J. Imrek,[18] M. Inaba,[68] D. Isenhower,[1] M. Ishihara,[57] T. Isobe,[13,57] M. Issah,[63,69] A. Isupov,[31] D. Ivanischev,[56] Y. Iwanaga,[24] B. V. Jacak,[64] J. Jia,[8,15,63] X. Jiang,[40] J. Jin,[15] B. M. Johnson,[8] T. Jones,[1] K. S. Joo,[48] D. Jouan,[54] D. S. Jumper,[1] F. Kajihara,[13] S. Kametani,[57] N. Kamihara,[58] J. Kamin,[64] J. H. Kang,[73] J. Kapustinsky,[40] K. Karatsu,[36,57] M. Kasai,[57,59] D. Kawall,[44,58] M. Kawashima,[57,59] A. V. Kazantsev,[35] T. Kempel,[29] A. Khanzadeev,[56] K. M. Kijima,[24] J. Kikuchi,[70] A. Kim,[20] B. I. Kim,[34] D. H. Kim,[48] D. J. Kim,[32,73] E. Kim,[62] E.-J. Kim,[11] S. H. Kim,[73] Y.-J. Kim,[26] E. Kinney,[14] K. Kiriluk,[14] Á. Kiss,[19] E. Kistenev,[8] J. Klay,[39] C. Klein-Boesing,[46] D. Kleinjan,[9] L. Kochenda,[56] B. Komkov,[56] M. Konno,[68] J. Koster,[26] A. Kozlov,[71] A. Král,[16] A. Kravitz,[15] G. J. Kunde,[40] K. Kurita,[57,59] M. Kurosawa,[57] M. J. Kweon,[34] Y. Kwon,[66,73] G. S. Kyle,[51] R. Lacey,[63] Y. S. Lai,[15] J. G. Lajoie,[29] D. Layton,[26] A. Lebedev,[29] D. M. Lee,[40] J. Lee,[20] K. B. Lee,[34] K. S. Lee,[34] T. Lee,[62] M. J. Leitch,[40] M. A. L. Leite,[61] B. Lenzi,[61] X. Li,[12] P. Lichtenwalner,[47] P. Liebing,[58] L. A. Linden Levy,[14] T. Liška,[16] A. Litvinenko,[31] H. Liu,[40,51] M. X. Liu,[40] B. Love,[69] D. Lynch,[8] C. F. Maguire,[69] Y. I. Makdisi,[7] A. Malakhov,[31] M. D. Malik,[50] V. I. Manko,[35] E. Mannel,[15] Y. Mao,[55,57] L. Mašek,[10,28] H. Masui,[68] F. Matathias,[15] M. McCumber,[64] P. L. McGaughey,[40] D. McGlinchey,[14,22] N. Means,[64] B. Meredith,[26] Y. Miake,[68] T. Mibe,[33] A. C. Mignerey,[43] P. Mikeš,[28] K. Miki,[57,68] A. Milov,[8] M. Mishra,[4] J. T. Mitchell,[8] A. K. Mohanty,[5] H. J. Moon,[48] Y. Morino,[13] A. Morreale,[9] D. P. Morrison,[8,†] T. V. Moukhanova,[35] D. Mukhopadhyay,[69] T. Murakami,[36] J. Murata,[57,59] S. Nagamiya,[33] J. L. Nagle,[14,‡] M. Naglis,[71] M. I. Nagy,[19,72] I. Nakagawa,[57,58] Y. Nakamiya,[24] K. R. Nakamura,[36,57] T. Nakamura,[24,57] K. Nakano,[57,67] S. Nam,[20] J. Newby,[39] M. Nguyen,[64] M. Nihashi,[24] T. Niida,[68] R. Nouicer,[8] A. S. Nyanin,[35] C. Oakley,[23] E. O'Brien,[8] S. X. Oda,[13] C. A. Ogilvie,[29] M. Oka,[68] K. Okada,[58] Y. Onuki,[57] A. Oskarsson,[42] M. Ouchida,[24,57] K. Ozawa,[13] R. Pak,[8] A. P. T. Palounek,[40] V. Pantuev,[27,64] V. Papavassiliou,[51] I. H. Park,[20] J. Park,[62] S. K. Park,[34] W. J. Park,[34] S. F. Pate,[51] H. Pei,[29] J.-C. Peng,[26] H. Pereira,[17] V. Peresedov,[31] D. Yu. Peressounko,[35] R. Petti,[64] C. Pinkenburg,[8] R. P. Pisani,[8] M. Proissl,[64] M. L. Purschke,[8] A. K. Purwar,[40] H. Qu,[23] J. Rak,[32,50] A. Rakotozafindrabe,[37] I. Ravinovich,[71] K. F. Read,[53,66] S. Rembeczki,[21] K. Reygers,[46] V. Riabov,[56] Y. Riabov,[56] E. Richardson,[43] D. Roach,[69] G. Roche,[41] S. D. Rolnick,[9] M. Rosati,[29] C. A. Rosen,[14] S. S. E. Rosendahl,[42] P. Rosnet,[41] P. Rukoyatkin,[31] P. Ružička,[28] V. L. Rykov,[57] B. Sahlmueller,[46,64] N. Saito,[33,36,57,58] T. Sakaguchi,[8] S. Sakai,[68] K. Sakashita,[57,67] V. Samsonov,[56] S. Sano,[13,70] T. Sato,[68] S. Sawada,[33] K. Sedgwick,[9] J. Seele,[14] R. Seidl,[26,58] A. Yu. Semenov,[29] V. Semenov,[25,27] R. Seto,[9] D. Sharma,[71] I. Shein,[25] T.-A. Shibata,[57,67] K. Shigaki,[24] M. Shimomura,[68] K. Shoji,[36,57] P. Shukla,[5] A. Sickles,[8] C. L. Silva,[29,61] D. Silvermyr,[53] C. Silvestre,[17] K. S. Sim,[34] B. K. Singh,[4] C. P. Singh,[4] V. Singh,[4] M. Slunečka,[10] A. Soldatov,[25] R. A. Soltz,[39] W. E. Sondheim,[40] S. P. Sorensen,[66] I. V. Sourikova,[8] F. Staley,[17] P. W. Stankus,[53] E. Stenlund,[42] M. Stepanov,[51] A. Ster,[72] S. P. Stoll,[8] T. Sugitate,[24] C. Suire,[54] A. Sukhanov,[8] J. Sziklai,[72] E. M. Takagui,[61] A. Taketani,[57,58] R. Tanabe,[68] Y. Tanaka,[49] S. Taneja,[64] K. Tanida,[36,57,58,62] M. J. Tannenbaum,[8] S. Tarafdar,[4] A. Taranenko,[63] P. Tarján,[18] H. Themann,[64] D. Thomas,[1] T. L. Thomas,[50] M. Togawa,[36,57,58] A. Toia,[64] L. Tomášek,[28] Y. Tomita,[68] H. Torii,[24,57] R. S. Towell,[1] V.-N. Tram,[37] I. Tserruya,[71] Y. Tsuchimoto,[24] C. Vale,[8,29] H. Valle,[69] H. W. van Hecke,[40] E. Vazquez-Zambrano,[15] A. Veicht,[26] J. Velkovska,[69] R. Vértesi,[18,72] A. A. Vinogradov,[35] M. Virius,[16] V. Vrba,[28] E. Vznuzdaev,[56] X. R. Wang,[51] D. Watanabe,[24] K. Watanabe,[68] Y. Watanabe,[57,58] F. Wei,[29] R. Wei,[63] J. Wessels,[46] S. N. White,[8] D. Winter,[15] C. L. Woody,[8] R. M. Wright,[1] M. Wysocki,[14] W. Xie,[58] Y. L. Yamaguchi,[13,57,70] K. Yamaura,[24] R. Yang,[26] A. Yanovich,[25] J. Ying,[23] S. Yokkaichi,[57,58] Z. You,[55] G. R. Young,[53] I. Younus,[38,50] I. E. Yushmanov,[35] W. A. Zajc,[15] O. Zaudtke,[46] C. Zhang,[53] S. Zhou,[12] and L. Zolin[31]

(PHENIX Collaboration)

[1]*Abilene Christian University, Abilene, Texas 79699, USA*
[2]*Institute of Physics, Academia Sinica, Taipei 11529, Taiwan*
[3]*Department of Physics, Augustana College, Sioux Falls, South Dakota 57197, USA*
[4]*Department of Physics, Banaras Hindu University, Varanasi 221005, India*
[5]*Bhabha Atomic Research Centre, Bombay 400 085, India*
[6]*Baruch College, City University of New York, New York, New York 10010, USA*
[7]*Collider-Accelerator Department, Brookhaven National Laboratory, Upton, New York 11973-5000, USA*
[8]*Physics Department, Brookhaven National Laboratory, Upton, New York 11973-5000, USA*
[9]*University of California - Riverside, Riverside, California 92521, USA*
[10]*Charles University, Ovocný trh 5, Praha 1, 116 36 Prague, Czech Republic*
[11]*Chonbuk National University, Jeonju 561-756, Korea*
[12]*Science and Technology on Nuclear Data Laboratory, China Institute of Atomic Energy, Beijing 102413, P. R. China*
[13]*Center for Nuclear Study, Graduate School of Science, University of Tokyo, 7-3-1 Hongo, Bunkyo, Tokyo 113-0033, Japan*
[14]*University of Colorado, Boulder, Colorado 80309, USA*
[15]*Columbia University, New York, New York 10027 and Nevis Laboratories, Irvington, New York 10533, USA*
[16]*Czech Technical University, Zikova 4, 166 36 Prague 6, Czech Republic*
[17]*Dapnia, CEA Saclay, F-91191 Gif-sur-Yvette, France*
[18]*Debrecen University, H-4010 Debrecen, Egyetem tér 1, Hungary*
[19]*ELTE, Eötvös Loránd University, H-1117 Budapest, Pázmány P. s. 1/A, Hungary*
[20]*Ewha Womans University, Seoul 120-750, Korea*
[21]*Florida Institute of Technology, Melbourne, Florida 32901, USA*
[22]*Florida State University, Tallahassee, Florida 32306, USA*
[23]*Georgia State University, Atlanta, Georgia 30303, USA*
[24]*Hiroshima University, Kagamiyama, Higashi-Hiroshima 739-8526, Japan*
[25]*IHEP Protvino, State Research Center of Russian Federation, Institute for High Energy Physics, Protvino 142281, Russia*
[26]*University of Illinois at Urbana-Champaign, Urbana, Illinois 61801, USA*
[27]*Institute for Nuclear Research of the Russian Academy of Sciences, prospekt 60-letiya Oktyabrya 7a, Moscow 117312, Russia*
[28]*Institute of Physics, Academy of Sciences of the Czech Republic, Na Slovance 2, 182 21 Prague 8, Czech Republic*
[29]*Iowa State University, Ames, Iowa 50011, USA*
[30]*Advanced Science Research Center, Japan Atomic Energy Agency, 2-4 Shirakata Shirane, Tokai-mura, Naka-gun, Ibaraki-ken 319-1195, Japan*
[31]*Joint Institute for Nuclear Research, 141980 Dubna, Moscow Region, Russia*
[32]*Helsinki Institute of Physics and University of Jyväskylä, P.O. Box 35, FI-40014 Jyväskylä, Finland*
[33]*KEK, High Energy Accelerator Research Organization, Tsukuba, Ibaraki 305-0801, Japan*
[34]*Korea University, Seoul 136-701, Korea*
[35]*Russian Research Center "Kurchatov Institute", Moscow 123098, Russia*
[36]*Kyoto University, Kyoto 606-8502, Japan*
[37]*Laboratoire Leprince-Ringuet, Ecole Polytechnique, CNRS-IN2P3, Route de Saclay, F-91128 Palaiseau, France*
[38]*Physics Department, Lahore University of Management Sciences, Lahore, Pakistan*
[39]*Lawrence Livermore National Laboratory, Livermore, California 94550, USA*
[40]*Los Alamos National Laboratory, Los Alamos, New Mexico 87545, USA*
[41]*LPC, Université Blaise Pascal, CNRS-IN2P3, Clermont-Fd, 63177 Aubiere Cedex, France*
[42]*Department of Physics, Lund University, Box 118, SE-221 00 Lund, Sweden*
[43]*University of Maryland, College Park, Maryland 20742, USA*
[44]*Department of Physics, University of Massachusetts, Amherst, Massachusetts 01003-9337, USA*
[45]*Department of Physics, University of Michigan, Ann Arbor, Michigan 48109-1040, USA*
[46]*Institut fur Kernphysik, University of Muenster, D-48149 Muenster, Germany*
[47]*Muhlenberg College, Allentown, Pennsylvania 18104-5586, USA*
[48]*Myongji University, Yongin, Kyonggido 449-728, Korea*
[49]*Nagasaki Institute of Applied Science, Nagasaki-shi, Nagasaki 851-0193, Japan*
[50]*University of New Mexico, Albuquerque, New Mexico 87131, USA*
[51]*New Mexico State University, Las Cruces, New Mexico 88003, USA*
[52]*Department of Physics and Astronomy, Ohio University, Athens, Ohio 45701, USA*
[53]*Oak Ridge National Laboratory, Oak Ridge, Tennessee 37831, USA*
[54]*IPN-Orsay, Universite Paris Sud, CNRS-IN2P3, BP1, F-91406 Orsay, France*
[55]*Peking University, Beijing 100871, P. R. China*
[56]*PNPI, Petersburg Nuclear Physics Institute, Gatchina, Leningrad Region 188300, Russia*
[57]*RIKEN Nishina Center for Accelerator-Based Science, Wako, Saitama 351-0198, Japan*
[58]*RIKEN BNL Research Center, Brookhaven National Laboratory, Upton, New York 11973-5000, USA*

[59]Physics Department, Rikkyo University, 3-34-1 Nishi-Ikebukuro, Toshima, Tokyo 171-8501, Japan
[60]Saint Petersburg State Polytechnic University, St. Petersburg 195251, Russia
[61]Universidade de São Paulo, Instituto de Física, Caixa Postal 66318, São Paulo CEP05315-970, Brazil
[62]Seoul National University, Seoul, Korea
[63]Chemistry Department, Stony Brook University, SUNY, Stony Brook, New York 11794-3400, USA
[64]Department of Physics and Astronomy, Stony Brook University, SUNY, Stony Brook, New York 11794-3800, USA
[65]SUBATECH (Ecole des Mines de Nantes, CNRS-IN2P3, Université de Nantes) BP 20722-44307, Nantes, France
[66]University of Tennessee, Knoxville, Tennessee 37996, USA
[67]Department of Physics, Tokyo Institute of Technology, Oh-okayama, Meguro, Tokyo 152-8551, Japan
[68]Institute of Physics, University of Tsukuba, Tsukuba, Ibaraki 305, Japan
[69]Vanderbilt University, Nashville, Tennessee 37235, USA
[70]Waseda University, Advanced Research Institute for Science and Engineering, 17 Kikui-cho, Shinjuku-ku, Tokyo 162-0044, Japan
[71]Weizmann Institute, Rehovot 76100, Israel
[72]Institute for Particle and Nuclear Physics, Wigner Research Centre for Physics, Hungarian Academy of Sciences (Wigner RCP, RMKI) H-1525 Budapest 114, P. O. Box 49, Budapest, Hungary
[73]Yonsei University, IPAP, Seoul 120-749, Korea

(Received 6 November 2013; published 31 March 2014)

Background: Heavy-flavor modification in relativistic $p(d) + A$ collisions are sensitive to different kinds of strong-interaction physics ranging from modifications of the nuclear wave function to initial- and final-state energy loss. Modifications to single heavy-flavor particles and their decay leptons at midrapidity and forward rapidity are well established at the Relativistic Heavy Ion Collider (RHIC).
Purpose: This paper presents measurements of azimuthal correlations of electron-muon pairs produced from heavy-flavor decays, primarily $c\bar{c}$, in $\sqrt{s_{NN}} = 200$ GeV $p + p$ and $d + $ Au collision using the PHENIX detector at RHIC. The electrons are measured at midrapidity while the muons in the pair are measured at forward rapidity, defined as the direction of the deuteron beam, in order to utilize the deuteron to probe low-x partons in the gold nucleus.
Methods: This analysis uses the central spectrometer arms for electron identification and forward spectrometer arms for muon identification. Azimuthal correlations are built in all sign combinations for e-μ pairs. Subtracting the like-sign yield from the unlike-sign yield removes the correlations from light flavor decays and conversions.
Results: Comparing the $p + p$ results with several different Monte Carlo event generators, we find the results are consistent with a total charm cross section $\sigma_{c\bar{c}} = 538 \pm 46$ (stat) ± 197 (data syst) ± 174 (model syst) μb. These generators also indicate that the back-to-back peak at $\Delta\phi = \pi$ is dominantly from the leading-order contributions (gluon fusion), while higher-order processes (flavor excitation and gluon splitting) contribute to the yield at all $\Delta\phi$. We observe a suppression in the pair yield per collision in $d + $ Au. We find the pair yield suppression factor for $2.7 < \Delta\phi < 3.2$ rad is $J_{dA} = 0.433 \pm 0.087$ (stat) ± 0.135 (syst).
Conclusions: The e-μ pairs result from partons at $x_{\mathrm{Au}} \sim 10^{-2}$ at $Q^2 = 10$ GeV$/c^2$ at the edge of the shadowing region. The pair suppression indicates modification to $c\bar{c}$ pairs for these kinematics in the cold nuclear medium at RHIC.

DOI: 10.1103/PhysRevC.89.034915 PACS number(s): 25.75.Dw, 25.75.Gz

I. INTRODUCTION

The study of open heavy-flavor production in relativistic $p(d) + A$ collisions is sensitive to different kinds of strong-interaction physics. Because the leading-order (LO) production mechanism is gluon fusion [1], open heavy-flavor production rates are directly related to modification of the gluon parton distribution function (PDF), i.e., shadowing or saturation [2]. Also, the initial- and/or final-state partons can scatter and lose energy in the cold nuclear medium [3–5], thereby modifying and producing a nuclear modification of open heavy-flavor production. Recently, the possibility of flow even in small collision systems such as $p(d) + A$ has raised the question of modified charm momentum distributions [6].

Modification to heavy quark production rates and kinematics in $d + $ Au collisions at the Relativistic Heavy Ion Collider (RHIC) is well established. Electron production from open heavy-flavor decay is enhanced [7], while J/ψ production [8] and Υ production [9] is suppressed at midrapidity. At positive rapidity, defined with the positive z axis as the direction of the deuteron, there is a suppression of heavy-flavor decay muons [10] and a larger suppression of J/ψ [8].

While e-μ correlations from open heavy-flavor decays have not been published at RHIC to date, correlations involving light flavor hadrons have shown modification in $d + $ Au collisions at RHIC. A suppression has been observed of positive rapidity

*Deceased.
†PHENIX Co-Spokesperson: morrison@bnl.gov
‡PHENIX Co-Spokesperson: jamie.nagle@colorado.edu

π^0 mesons associated with midrapidity trigger hadrons, especially in the back-to-back peak at $\Delta\phi = \pi$, indicating $2 \to 2$ scatterings [11,12]. This suppression increases as x, the fraction of the nucleon momentum carried by the gluon, decreases. These results are in quantitative agreement with energy-loss models [13] and saturation models [14–16].

This paper presents measurements of azimuthal correlations of electron-muon pairs produced from heavy-flavor decays, primarily $c\bar{c}$, in $p+p$ and $d+\mathrm{Au}$ collisions using the PHENIX detector at RHIC. The heavy-flavor e-μ correlations are free of backgrounds from other sources that contribute to other dilepton analyses (e^+e^- or $\mu^+\mu^-$), such as resonance decay and Drell-Yan. While analysis of dilepton mass and p_T provides a way to separate charm and bottom contributions, the azimuthal correlations have an important advantage for studying the charm production process. The leading-order production, $gg \to Q\bar{Q}$ and $q\bar{q} \to Q\bar{Q}$, will produce back-to-back open heavy-flavor pairs that can semileptonically decay and produce azimuthally correlated e-μ pairs. Next-to-leading-order (NLO) processes like flavor excitation and gluon splitting produce much less correlated $Q\bar{Q}$ and thus much less correlated e-μ pairs. Therefore, modification to different portions of the azimuthal correlations can be attributed to modifications of $c\bar{c}$ pairs from different production mechanisms. In energy loss models such as Ref. [13], a broadening of the back-to-back azimuthal correlation should accompany a suppression of the peak due to the multiple scattering that the incoming gluons and/or the outgoing $c\bar{c}$ undergo in the cold nuclear medium.

This paper is organized as follows. The PHENIX detector is outlined in Sec. II. Section III describes the details of the method used to measure the correlations, the background subtraction method, and the tests of the method. Section IV presents the results in $p+p$ and compares them to Monte Carlo models. The $d+\mathrm{Au}$ results are presented and compared to the $p+p$ results in Sec. IV B. Conclusions are given in Sec. V.

II. PHENIX EXPERIMENT

The PHENIX detector at RHIC is multipurposed and optimized for precision measurements of electromagnetic probes for relativistic hadronic and heavy-ion collisions. A complete overview of the detector can be found in Ref. [17]. The data presented here are from 2006 $p+p$ and 2008 $d+\mathrm{Au}$ data taking at RHIC. Figure 1 shows a schematic of the detector during those years. This analysis uses the central spectrometer arms for electron detection and the forward rapidity muon spectrometer arms, labeled North and South in Fig. 1, for muon identification. For the 2008 $d+\mathrm{Au}$ collisions, the deuteron beam moves toward the North arm, which defines positive rapidity for both $p+p$ and $d+\mathrm{Au}$. The forward produced muons come from a high-x parton in the deuteron interacting with a low-x parton in the gold. PYTHIA [18] indicates that the average x of a parton producing a heavy-flavor muon from $1 < p_T^{\mu} < 6\ \mathrm{GeV}/c$ in the forward muon spectrometer is about 5×10^{-3}. This analysis focuses only on the muons measured in the North arm utilizing the deuteron beam as a probe of low-x partons in the gold nucleus.

The central spectrometer comprises two arms subtending $\pi/2$ in azimuth and covering $|\eta| < 0.35$. Charged tracks are measured using a drift chamber (DC) and a set of multiwire proportional chambers with pad readout (PC1 and PC3). The DC measures the bend angle in the r-ϕ plane due to a central magnetic field directed along the beam axis. PC1 is used to measure the longitudinal coordinate of the track. These tracks are then projected into PC3, where a hit is required to ensure high track quality. The momentum resolution of the tracks in this data is $\delta p/p = 1.10\% \oplus 1.16\% p$, where p is the total momentum measured in GeV/c. Electrons can be identified from associated hits in the Ring Imaging Čerenkov (RICH) detector and the Electromagnetic Calorimeters (EMCal). Electrons above 17 MeV/c passing through the CO_2-filled RICH will emit Čerenkov radiation. The EMCal comprises eight sectors, six of lead-scintillator and two of lead-glass, used to collect the energy from electron and photon showers. The nominal energy resolution for the lead-scintillator and lead-glass is $8.1\% \pm \sqrt{E[\mathrm{GeV}]} \oplus 2.1\%$ and $6.0\% \pm \sqrt{E[\mathrm{GeV}]} \oplus 0.9\%$ [19], respectively.

The North muon spectrometer is located at $1.2 < \eta < 2.4$ and covers 2π in azimuth. The spectrometer measures tracks in the muon tracker (MuTr) and the muon identifier (MuID). Prior to entering the muon arm, particles pass through approximately 20 cm of copper and 60 cm of iron. Particles that are not absorbed pass through the MuTr, which comprises three stations of cathode strip chambers with multiple ionization regions and located inside a radial magnetic field. After the MuTr, particles pass through the MuID, which comprises five alternating steel absorbers and MuID detector planes, called gaps, with Iarocci tubes. MuID roads reconstructed from MuID hits are projected back to MuTr tracks and to the measured vertex to provide the complete information for a track through the spectrometer.

Trigger and global event characterization in $p+p$ and $d+\mathrm{Au}$ are provided by the beam-beam counter (BBC). The BBC is a set of 64 hexagonal Čerenkov counters located from $3.0 < |\eta| < 3.9$ and covering full azimuth. The vertex of the collision along the beam line (z_{vtx}) is determined by the time difference between the BBCs on either side of the collision region. The minimum bias (MB) trigger requires that there is at least one hit in each of the BBCs. From Vernier scans and verified by Monte Carlo studies, the BBC MB trigger is sensitive to $55 \pm 5\%$ of the $p+p$ inelastic cross section and $88 \pm 4\%$ of the $d+\mathrm{Au}$ inelastic cross section [20]. The trigger used for this analysis is a combination of the BBC trigger and a deep muon trigger. The deep muon trigger requires three or more MuID gaps with a signal in both the x and y direction tubes and that the last pair of hits be in the last (fifth gap) or next to last gap (fourth gap).

After quality cuts and requiring a vertex within 25 cm of the $z = 0$ vertex, an integrated luminosity of 2.1 pb^{-1} in $p+p$ and a $p+p$ equivalent of 7.7 pb^{-1} in $d+\mathrm{Au}$ was sampled.

III. ANALYSIS

The primary goal of this analysis is to identify

$$p + p(d + \mathrm{Au}) \to c\bar{c} + X \to e^{\pm}\mu^{\mp} + X, \qquad (1)$$

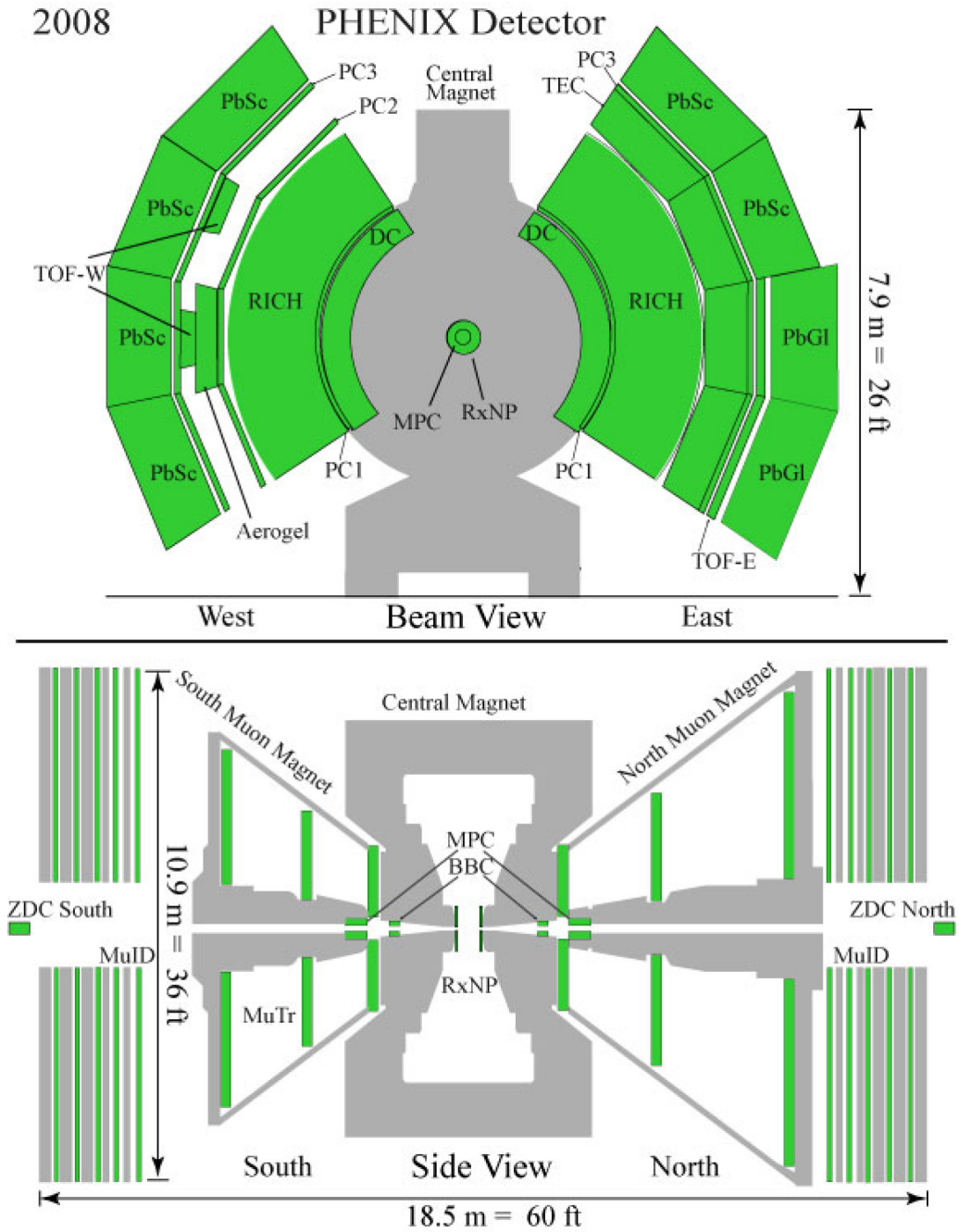

FIG. 1. (Color online) A schematic view of the PHENIX detector during the 2008 $d + \mathrm{Au}$ data taking. (a) Beam view of the central spectrometer arms. (b) Longitudinal view including the global event and triggering detectors, as well as the muon spectrometer arms. The configurations of the central spectrometer and muon arms were the same for the 2006 $p + p$ data taking.

where the opposite-sign electron-muon pair is from the $c\bar{c}$ pair decay.

A. Particle identification

1. Muon identification

Real muons with total momentum less than $\approx$2.7 GeV/c are stopped in the muon arm before reaching the fifth (and last) gap. We apply an additional cut on muons with $p_T < 1$ GeV/c to avoid a region with larger backgrounds and near the acceptance edge. Single muon candidates are constructed from MuID roads projected and matched to MuTr tracks. Cuts on MuID roads and MuTr tracks are designed to reject hadrons that mimic a muon signal and to reject tracks that did not originate from the collision vertex. For the MuID roads, at least three of five gaps with x-y hit information are required, including a pair of hits in the fifth gap. These MuID roads must project back near the nominal vertex position, thus selecting muons that do not typically come from beam-related backgrounds. For the MuTr tracks, cuts that reject hadrons are

detailed in Ref. [21]. The MuID roads are then projected and matched to MuTr tracks at the first MuID gap. An identified muon candidate is the closest MuTr track that matches a MuID road within at least 10° in slope and 10 cm in distance. Muon candidates are further restricted to $1.4 < \eta < 2.1$. During both the $p + p$ and $d + \mathrm{Au}$ data taking periods, there were backgrounds primarily from beam-related particles interacting with material in the accelerator upstream of PHENIX, which varied throughout the running period. Collimators were used in the accelerator to reduce this background, but it was not totally eliminated. However, restricting the η range of the muon candidates helped to minimize this background. The analysis was divided into several run groups to assess this and other similar systematic errors. The fully corrected yields for the different run groups varied within 2%.

2. *Electron identification*

Electrons with $p_T > 0.5\ \mathrm{GeV}/c$ are identified by matching a track in DC, PC1, and PC3 to a signal in the RICH and a cluster in the EMCal. The relevant details on measuring electrons in PHENIX are given in Ref. [22]. For this analysis, the projected track must match within 3σ in position to a cluster in the EMCal. Clusters are also required to have a matching profile, when compared to an electromagnetic shower shape profile at the measured energy. Once a track matches both the RICH and the EMCal, an E/p cut is applied, where it is required that the energy measured in the the EMCal E be approximately equal to the reconstructed track momentum p. This is sufficient to remove most combinatorial matches and background from real electrons resulting from long-lived particle decays occurring near the DC, which have mismeasured momentum. A cut of -2σ to $+3\sigma$ from the mean E/p in the $p + p$ data and -1.5σ to $+3\sigma$ from the mean in the $d + \mathrm{Au}$ data is applied. The asymmetry of the cuts is due to the dominance of backgrounds below 2 or 1.5σ of the mean. The tighter cut in the $d + \mathrm{Au}$ data was necessary because of the increased background from the hadron blind detector (HBD) support material not present during 2006 data taking.

B. Acceptance and efficiencies

After particle identification cuts have been applied to an event, all pairs of identified electrons and muons are formed in each of the four charge-sign combinations. The fully corrected invariant-pair yield, calculated for each sign combination, is [23]

$$\frac{d^3N}{dy^\mu dy^e d\Delta\phi} = \frac{c}{N_{\mathrm{evt}}^{\mathrm{MB}} \Delta y^e \Delta y^\mu \Delta\phi^{\mathrm{bin}}} \frac{\int d\Delta\phi \mathrm{Mix}(\Delta\phi)}{2\pi} \times \frac{N^{e\mu}(\Delta\phi)}{\mathrm{Mix}^{e\mu}(\Delta\phi,\epsilon^e,\epsilon^\mu)}, \quad (2)$$

where $N_{\mathrm{evt}}^{\mathrm{MB}}$ is the number of sampled BBC triggered events; c is the MB trigger bias accounting for events missed by the BBC trigger [20]; Δy^e and Δy^μ are the rapidity ranges of the electrons and muons, respectively; $N^{e\mu}(\Delta\phi)$ is the inclusive electron-muon pair yield; and $\mathrm{Mix}^{e\mu}(\Delta\phi,\epsilon^e,\epsilon^\mu)$ is the mixed-event electron-muon pair distribution. The two-particle acceptance times efficiency is corrected by the mixed-event technique, where electrons from one event are paired with muons from a different event. Pools of inclusive electrons and muons are kept in 2.5-cm-wide z-vertex bins and, in the case of $d + \mathrm{Au}$, 10%-wide centrality bins. When mixing events, the pair distribution is weighted by the y- and ϕ-averaged efficiency of each particle, ϵ^e and ϵ^μ.

Both ϵ^e and ϵ^μ were determined by generating single electrons and single muons with a flat distribution in p_T, ϕ, $|y^e| < 0.5$ or $1.4 < y^\mu < 2.2$ and collision z-vertex location and running them through a GEANT-3 simulation of the PHENIX detector. The output was weighted with the PHENIX single lepton p_T spectra and then subjected to the same analysis cuts applied to the data. The efficiency is defined as the ratio of particles reconstructed through the analysis to the number simulated. These simulations demonstrated that ϵ^e and ϵ^μ are independent of the z position of the event vertex, ϵ^e is independent of η, and ϵ^μ has a slight η dependence. Pair yields are reported with the average pseudorapidity $\langle\eta^\mu\rangle$, which include the η dependence of both single inclusive muons and the single-particle efficiency.

C. Background subtraction

Inclusive muon and electron candidates come from both heavy- and light-flavor decays and from misidentified hadrons. The fully corrected inclusive electron-muon pair yield for each sign combinations can be written as

$$N^{e\mu}(\Delta\phi) = N_H^{e\mu}(\Delta\phi) + N_{LH}^{e\mu}(\Delta\phi) + N_L^{e\mu}(\Delta\phi). \quad (3)$$

Here $N^{e\mu}$ indicates the fully corrected inclusive pair yield defined in Eq. (2); $N_H^{e\mu}(\Delta\phi)$ is the fully corrected pair yield produced from a heavy-flavor pair decay; $N_{LH}^{e\mu}(\Delta\phi)$ is the fully corrected pair yield from correlating a heavy-flavor decay product with a light flavor decay product; and $N_L^{e\mu}(\Delta\phi)$ is the fully corrected pair yield from correlating pairs of light-flavor decay products or misidentified hadrons. Pairs from the semileptonic decay of a $c\bar{c}$ pair have opposite signs. Equation (3) can be decomposed into its like- and unlike-sign pieces as follows:

$$\begin{aligned} N_{\mathrm{like}}^{e\mu}(\Delta\phi) &= N_{LH,\mathrm{like}}^{e\mu}(\Delta\phi) + N_{L,\mathrm{like}}^{e\mu}(\Delta\phi) \\ N_{\mathrm{unlike}}^{e\mu}(\Delta\phi) &= N_{H,\mathrm{unlike}}^{e\mu}(\Delta\phi) + N_{LH,\mathrm{unlike}}^{e\mu}(\Delta\phi) \\ &\quad + N_{L,\mathrm{unlike}}^{e\mu}(\Delta\phi). \end{aligned} \quad (4)$$

While semileptonic decays of $b\bar{b}$ can also produce both like- and unlike-sign e-μ signals, in this analysis, PYTHIA indicates that only about 1% of the final heavy-flavor e-μ pair yield is from $b\bar{b}$ and is neglected. If we assume muon (electron) candidates from light flavors are not charge correlated with electron (muon) candidates from light flavors, then

$$N_{L,\mathrm{like}}^{e\mu}(\Delta\phi) = N_{L,\mathrm{unlike}}^{e\mu}(\Delta\phi). \quad (5)$$

If only one of the pair is from heavy flavor, then, again, we assume they are not charge correlated and

$$N_{LH,\mathrm{like}}^{e\mu}(\Delta\phi) = N_{LH,\mathrm{unlike}}^{e\mu}(\Delta\phi). \quad (6)$$

Therefore, the heavy-flavor e-μ signal distribution is the difference between the unlike-sign and the like-sign inclusive

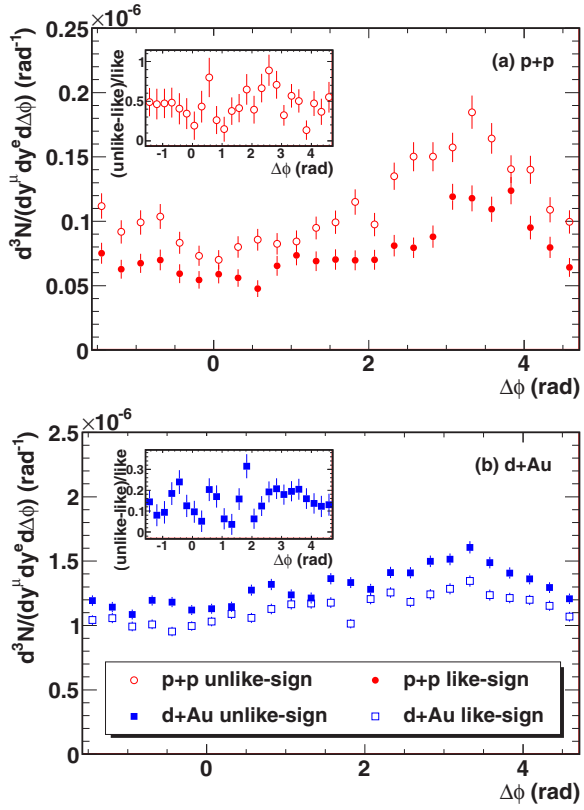

FIG. 2. (Color online) The fully corrected inclusive like-sign ($e^{\pm}$-$\mu^{\pm}$) and unlike-sign ($e^{\pm}$-$\mu^{\mp}$) distributions for (a) $p+p$ and (b) $d+\mathrm{Au}$ as a function of $\Delta\phi$. The inset shows the unlike-like difference divided by the like-sign distribution, which is the heavy-flavor signal-to-background in the inclusive unlike-sign distribution.

correlations as follows:

$$N_H^{e\mu}(\Delta\phi) = N_{\mathrm{unlike}}^{e\mu}(\Delta\phi) - N_{\mathrm{like}}^{e\mu}(\Delta\phi). \tag{7}$$

Figure 2 shows the fully corrected inclusive like-sign $[N_{\mathrm{like}}^{e\mu}(\Delta\phi)]$ and unlike-sign $[N_{\mathrm{unlike}}^{e\mu}(\Delta\phi)]$ e-μ pair distributions in $p+p$ and $d+\mathrm{Au}$. The inset figures show the signal-to-background distributions given the assumptions above.

We have checked the like-sign subtraction method using PYTHIA leading-order quantum chromodynamics (QCD) events. With all events containing a heavy quark in the final state removed, the pair yields as a function of $\Delta\phi$ for like-sign and unlike-sign electron-muon pairs were the same within 3% over all $\Delta\phi$.

While this corroborates the basic idea of the subtraction, the assumption was further tested with data. In the following sections we detail the results of different methods to tag electrons and muons from light flavor decay to examine the validity of Eq. (7) and to quantify the systematic uncertainty of the method. The general method is to use a sample of single electrons paired with single muons, where one or both are likely from light-hadron decays. If the method is correct, the like-sign subtraction should produce no correlation at all. If there are statistically significant correlations after like-sign subtraction, these are subtracted from the final e-μ pair yield and uncertainties on the residual correlation strength

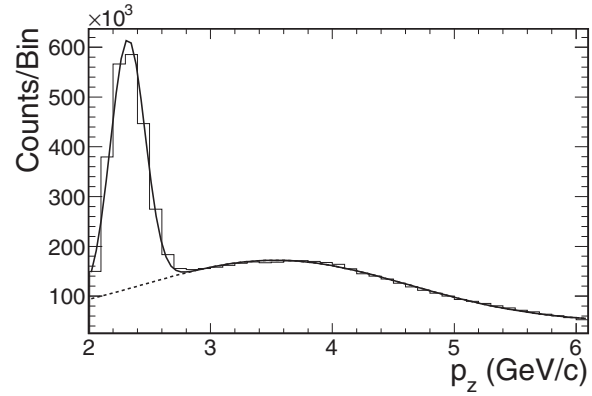

FIG. 3. The distribution of p_z for tracks that stop in the next-to-last MuID gap (fourth gap). The peak at lower p_z is due to muons, while the broad distribution is from hadrons that punch through the absorber to the fourth gap. The solid line is a two-Gaussian fit to this distribution with the solid line indicating the hadronic background in the muon peak region.

are propagated as a systematic uncertainty on the final pair yield. If no statistically significant yield is found after like-sign subtraction, the statistical uncertainty on the zero yield is propagated as the systematic uncertainty.

1. *Correlations between inclusive electrons and punch-through hadrons that fake single muons*

One source of background to the single muons is from hadrons that penetrate to the fifth gap, called punch-through hadrons. After single-particle cuts there is some small fraction (roughly 1 of every 250 [24]) of candidate tracks with $p_T > 1$ GeV/c that are hadrons that punch through. While this represents an irreducible background to the single muons, we can obtain a clean sample of hadrons that punch through and stop in the fourth gap of the MuID. Figure 3 shows the p_z distribution of muon candidates that stop in the fourth gap. The peak at 2.3 GeV/c is composed of muons that have insufficient energy to penetrate further. The broader portion of the distribution comprises light hadrons that are not stopped by the upstream absorber materials but are subsequently absorbed in the steel just after the fourth gap, thus not leaving a hit in the fifth gap. We identify punch-through hadrons as having stopped in the fourth gap with p_z larger than 3 GeV/c.

Figure 4 shows the fully corrected like-sign-subtracted pair yield of central-arm electrons and the punch-through hadrons in the muon arms for both $p+p$ and $d+\mathrm{Au}$ collisions. If both the like- and unlike-sign pair yields were dominantly from light-hadron decays, the like-sign subtraction should produce zero pair yield. To determine the magnitude of the residual correlation strength after like-sign subtraction, the $p+p$ data were fitted with a flat line. This is shown as the solid line in Fig. 4(a). The fit uncertainty is shown as the shaded band around the solid line. The flat fit in $p+p$ had a χ^2 per number of degrees of freedom (NDF) of 22.7/24 and gave a value that was nonzero with greater than 1σ significance. This means there is yield in the final e-μ correlations from these punch-through hadrons. The fitted yield was subtracted from the final

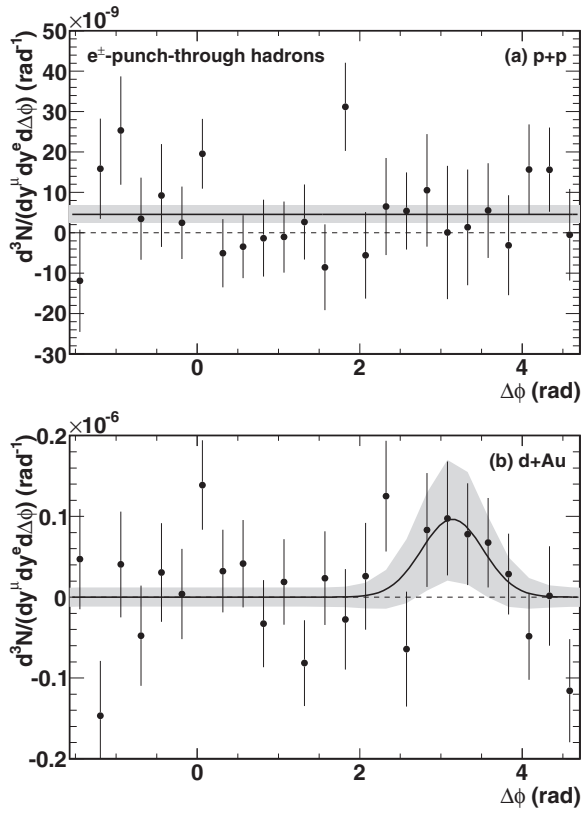

FIG. 4. The fully corrected like-sign-subtracted electron plus punch-through hadron pair yield in (a) $p+p$ and (b) $d+\mathrm{Au}$ collisions. The (a) solid line and (b) solid curve are the fitted yields that are removed from the inclusive electron-muon pair correlation. The shaded bands indicate the fit uncertainty that is propagated as a systematic uncertainty in the final pair yield. In (a) $p+p$, the fit is a flat line with $\chi^2/\mathrm{NDF} = 22.7/24$. In (b) $d+\mathrm{Au}$, the fit is a flat line and a Gaussian centered at π with $\chi^2/\mathrm{NDF} = 26.3/22$.

pair yield and its uncertainty was propagated as a systematic uncertainty on the final pair yield. For the $d+\mathrm{Au}$ case, we fitted the residual correlation to a flat line and found reasonable agreement with a χ^2/NDF of 30.9/24 or a p value of 14%. However, there is a possible excess of counts near $\Delta\phi = \pi$, which when included as a Gaussian component fixed at $\Delta\phi = \pi$ and the width and yield as free parameters, a slightly better χ^2/NDF of 26.3/22 or a p value of 26% was found. If there is any correlated yield beyond a pedestal, it would show up in the back-to-back peak. Therefore, we subtract the Gaussian fit, shown as the solid curve in Fig. 4 from the final pair yield, and propagate the uncertainty on the fit, shown as the shaded region around the solid curve, to the systematic uncertainty in the final pair yield.

Two additional corrections to this data are applied before subtraction from the final pair yield. Because the punch-through hadrons are measured in the fourth gap, the yields need to be scaled to match the rate of hadrons at the last gap. The rate of hadrons at the fifth gap was determined by using pion and kaon NLO perturbative QCD spectra [25] and passing them through a GEANT-3 model of the PHENIX muon arms. The MuID absorber steel cross section was modified until there was agreement between data and the simulation for the rate of punch-through hadrons in the third and fourth gap. We extrapolated to the fifth gap and find the rate of hadrons is 2.81 ± 0.30 times the rate of punch-through hadrons in the fourth gap [21]. The 3 GeV/c p_z cut removes some fraction of the punch-through hadrons. Based on the two-component fit to the p_z distribution shown in Fig. 3, the yield is scaled up to account for those hadrons rejected by the p_z cut. In the end, the pair yield uncertainty is 2.17×10^{-9} $(\mathrm{rad})^{-1}$ in $p+p$. In $d+\mathrm{Au}$ there is a $\Delta\phi$-independent uncertainty on the final pair yield that is 1.42×10^{-8} $(\mathrm{rad})^{-1}$ and the Gaussian uncertainty that ranges from 0 to 6.30×10^{-8} $(\mathrm{rad})^{-1}$.

2. *Correlations between inclusive electrons and light-hadron decay muons*

One source of real muons is from decays of light hadrons before and in the absorber material. These decay muons are predominantly from pions and kaons that are either directly produced in the collision or the result of low-mass resonance decays. The observed rate of muons into the North arm is higher, when the collision vertex is farther from the spectrometer arm. Because heavy-flavor decays (including Drell-Yan, heavy quarkonia, etc.) have a much shorter $c\tau$ than light flavor decays, heavy-flavor decay muons have a much weaker vertex dependence. Therefore, we assume there are two components to the muon rate: a component that follows the primary vertex distribution, attributable to heavy-flavor decays, and a component that folds the linear component due to light-hadron decays with the primary vertex distribution.

Muons from events that are near the detector ($0 < z_{\mathrm{vtx}} < 30$ cm) and far from the detector ($-30 < z_{\mathrm{vtx}} < 0$ cm), where z_{vtx} is the measured collisions vertex, are separately correlated with central arm electrons. Because the signal heavy-flavor muons follow the primary collision vertex distribution, subtracting the near-vertex pair yield from the far-vertex pair yield, should remove these and only residual correlations from decay muons should be present. The pair yields in $p+p$ and $d+\mathrm{Au}$ after subtracting near- and far-vertex muons and after like-sign subtraction are shown in Fig. 5. The $d+\mathrm{Au}$ correlations are consistent with a flat line with zero yield with a χ^2/NDF of 18.0/24. The $p+p$ data are not exactly flat at zero yield. However, this shape is not seen in $d+\mathrm{Au}$ and is not symmetric about $\Delta\phi = 0$ or $\Delta\phi = \pi$, so it is not related to physics. Therefore, we fit with a flat line that results in zero correlation yield and a χ^2/NDF of 27.1/24 corresponding to a p value of 30%. The fits are shown in Fig. 5 as solid lines and shaded bands, indicating the statistical uncertainties. These uncertainties were propagated into the systematic uncertainties of the final pair yields.

To propagate the uncertainties, additional corrections are needed. First, in the far-near subtraction, some fraction of the decay muons are removed. Second, light-hadron decays outside the ±30-cm vertex cut are not counted in the subtraction. To account for both effects, a fit to the vertex dependence of the muon yield is extrapolated to a point one interaction length inside the absorber, a distance of about 56 cm from the nominal z vertex and about 16 cm into the absorber. It is assumed that the decay contribution to the muons is negligible at that point,

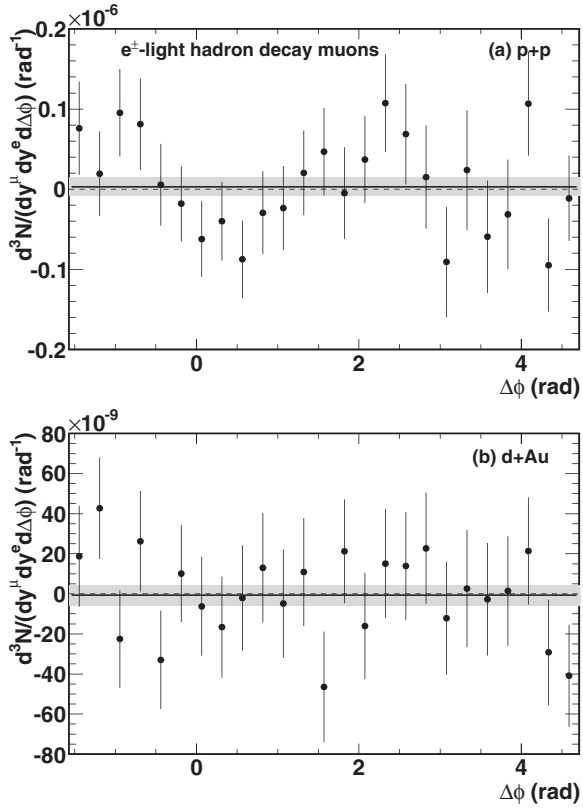

FIG. 5. The fully corrected like-sign-subtracted and near-far vertex-subtracted (see text) muon-decay $\Delta\phi$ pair yield in (a) $p + p$ and (b) $d + \mathrm{Au}$ collisions. Both are consistent with no residual correlation after like-sign subtraction. The solid lines and shaded bands indicate the flat line fits and their uncertainty with χ^2/NDF of 27.1/24 and 18.0/24 in (a) $p + p$ and (b) $d + \mathrm{Au}$, respectively.

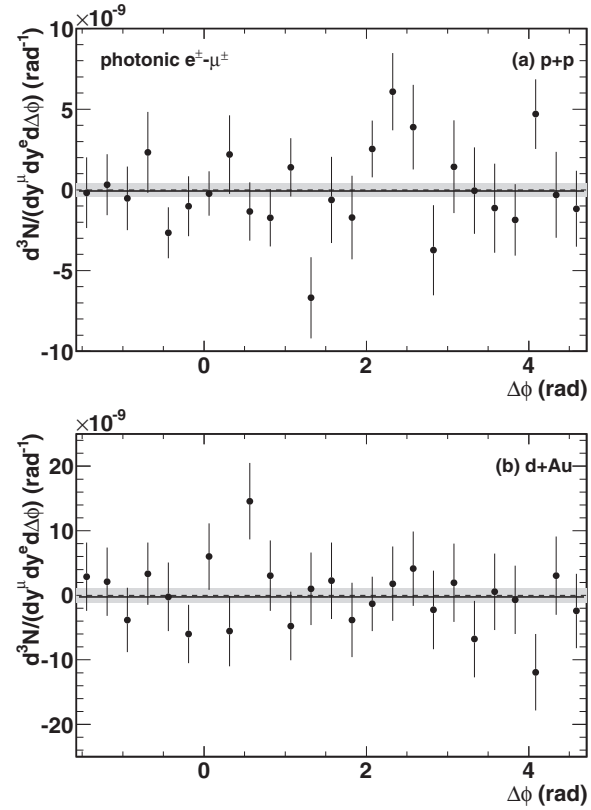

FIG. 6. The fully corrected like-sign-subtracted photonic electron-muon $\Delta\phi$ pair yield in (a) $p + p$ and (b) $d + \mathrm{Au}$ collisions. Both are consistent with no residual correlation after like-sign subtraction. The solid lines and shaded bands indicate the flat line fits and their uncertainties with χ^2/NDF of 33.2/24 and 20.2/24 in $p + p$ and $d + \mathrm{Au}$, respectively.

which fixes the fraction of muons that are from light decays within the measured vertex window of the analysis. Under this assumption, only 22% of the decay muons are measured within the vertex window after the like-sign subtraction. The fit uncertainties are increased to account for those muons not measured. The final systematic uncertainties on the final pair yield are 1.13×10^{-8} $(\mathrm{rad})^{-1}$ and 5.05×10^{-8}, independent of $\Delta\phi$ for $p + p$ and $d + \mathrm{Au}$, respectively.

3. *Correlations between photonic electrons and inclusive muons*

Electrons can result from light-hadron decays. The dominant photonic source of electrons are from π^0 decays, either directly by Dalitz decay or from conversions of the decay photons in detector material. We assume that if we measure the π^0-decay electrons correlations with muons, this will represent the other photonic sources (such as η and ω decay) in shape and yield. To tag decay or converted electrons, we construct the invariant mass distribution of all pairs of electrons and photons in an event. Electrons paired with photons within the π^0 mass peak are then correlated with muon candidates. The signal-to-background of pairs in the π^0 mass range is about 1. To remove correlations from combinatorial electron-photon pairs that fall within the π^0 mass window, muon candidates were also correlated with the e-γ pairs in a "sideband" π^0 mass region from 0.2 to 0.4 GeV/c^2. After scaling by the appropriate signal-to-background under the π^0 mass region, the "sideband" correlations were subtracted from the in-mass electron-muon correlations for each of the e-μ charge types.

Figure 6 shows the "sideband" -subtracted and like-sign-subtracted correlation between electrons tagged in the π^0 mass region with muons from $p + p$ and $d + \mathrm{Au}$ data. Flat fits to these correlations produced a yield consistent with zero with χ^2/NDF of 33.2/24 and 20.2/24 in $p + p$ and $d + \mathrm{Au}$ data, respectively. The statistical uncertainty from the fitted yield to the π^0-tagged correlations is a factor of 10 smaller than the other background correlations after accounting for reconstruction efficiency and additional sources of photonic electrons. This uncertainty is negligible compared to those from the muon backgrounds.

D. Systematic uncertainties

In this analysis there are three general types of uncertainty that we identify as type A (point-to-point uncorrelated), type B (point-to-point but correlated), and type C (total normalization uncertainty). Except for statistical uncertainties there are no type A uncertainties in this analysis.

TABLE I. Table of type B and type C systematic uncertainties for $p+p$ and $d+$Au collision data. The uncertainties on the muon and electron cuts are highly correlated between $p+p$ and $d+$Au.

Type	Description	$p+p$	$d+$Au
B	$\Delta\phi$ dependent	–	0 to 6.30×10^{-8}(rad)$^{-1}$
B	Punch-through	2.17×10^{-9} (rad)$^{-1}$	1.42×10^{-8}(rad)$^{-1}$
B	Decay muons	1.13×10^{-8} (rad)$^{-1}$	5.05×10^{-8}(rad)$^{-1}$
C	Muon cuts	7.8%	8.3%
C	Electron cuts	8.3%	9.3%
C	Muon efficiency	2.2%	2.2%
C	Electron efficiency	1.0%	1.0%
C	Trigger efficiency	11.1%	4.2%
C	Total	16.1%	13.4%

The type B uncertainties are from the subtraction of known backgrounds discussed in Sec. III C. The fully corrected pair yield uncertainties in $p+p$ are 2.17×10^{-9} (rad)$^{-1}$ and 1.13×10^{-8} (rad)$^{-1}$ from punch-through hadron and decay hadron subtraction uncertainties, respectively. These values are independent of $\Delta\phi$. In $d+$Au the flat-line fit contributions to the systematic uncertainty are 1.42×10^{-8} (rad)$^{-1}$ and 5.05×10^{-8} (rad)$^{-1}$ from punch-through hadron and decay hadron subtraction uncertainties, respectively. The additional uncertainty from the Gaussian fit to the punch-through hadron correlations resulted in a $\Delta\phi$-dependent uncertainty ranging in absolute value of 0 at $\Delta\phi\sim2$ rad to 6.30×10^{-8} (rad)$^{-1}$ at $\Delta\phi\sim\pi$. The type B systematic uncertainties are summarized in Table I.

The type C uncertainties are attributable to several sources and are given in Table I. One source of systematic uncertainty is evaluated by tightening the single-particle cuts for this analysis. Each single-particle cut was tightened independently and the analysis, including reevaluation of the single-particle efficiency, was performed. The uncertainty from each of the individual single-particle cuts was combined using the correlation among the cuts. The values of these are different in $p+p$ and $d+$Au data, because of the higher backgrounds in $d+$Au collisions. However, these uncertainties are highly correlated between $p+p$ and $d+$Au, because the same cuts are applied to both data sets. Another source of uncertainty is in the evaluation of the single-particle efficiencies. The single particles were generated flat in p_T and then weighted to match the measured PHENIX heavy-flavor lepton spectra [26]. For the uncertainty determination, the single-particle efficiency was re-evaluated without the weighting applied. This was estimated to be 1.0% for the electrons and 0.8% for the muons. For muons there is an additional 2.0% uncertainty due to the run-by-run variation in muon acceptance. The final portion of the type C systematic uncertainty is due to the trigger efficiency. To evaluate this uncertainty, the data were analyzed for several data-taking periods defined by the muon trigger performance. The difference in fully corrected yields between data sets was taken to be the uncertainty in the muon trigger efficiency. This is combined with the uncertainties in the bias factor c in Eq. (2). The total uncertainty for the trigger is 11.1% for $p+p$ and 4.2% for $d+$Au. As indicated in Table I, combining all type C uncertainties gives 16.1% for $p+p$ data and 13.4% for $d+$Au data.

IV. RESULTS

A. Pair yields for $p+p$ data and comparison with Monte Carlo generators

The fully corrected like-sign-subtracted e-μ pair yield as a function of $\Delta\phi$ for electrons with $p_T>0.5$ GeV/c and $|\eta|<0.5$, with opposite-signed forward muons with $p_T>1.0$ GeV/c and $1.4<\eta<2.1$, in $p+p$ is shown in Fig. 7. The average muon η in these correlations is 1.75. The error bars are statistical uncertainties only, while the boxes are the type B systematic uncertainties. We note that the distribution has two components: a nonzero continuum as well as a back-to-back peak near $\Delta\phi=\pi$.

To interpret these data, we compare the $p+p$ results to several different Monte Carlo event generators, PYTHIA, POWHEG [27], and MC@NLO [28].

The PYTHIA MB QCD events were generated to model the LO gluon fusion process and also model next-to-leading-order processes, like flavor excitation and gluon splitting. The parameters used to generate these events are the same as those used in Ref. [29]. Events with a $c\bar{c}$ pair and an electron and a muon in the measured kinematic range as the corrected data ($p_T^e>0.5$ GeV/c and $|\eta^e|<0.5$, $p_T^\mu>1$ GeV/c and $1.4<\eta^\mu<2.1$) were correlated and a like-sign subtraction

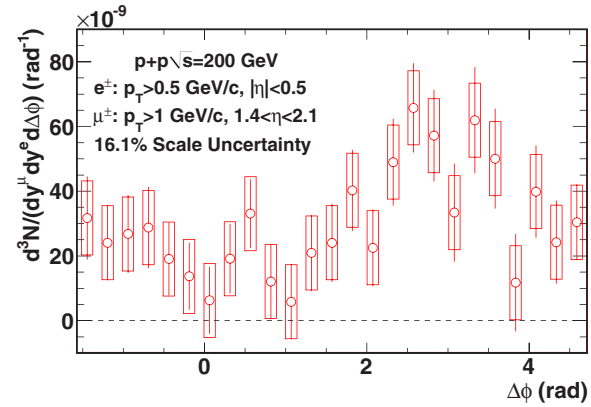

FIG. 7. (Color online) The fully corrected like-sign-subtracted heavy-flavor e-μ pair yield in $p+p$. The error bars are statistical only. The boxes show the type B systematic uncertainty from the punch-through hadron and light-hadron-decay muon-background subtraction. The 16.1% type C systematic uncertainty is not shown.

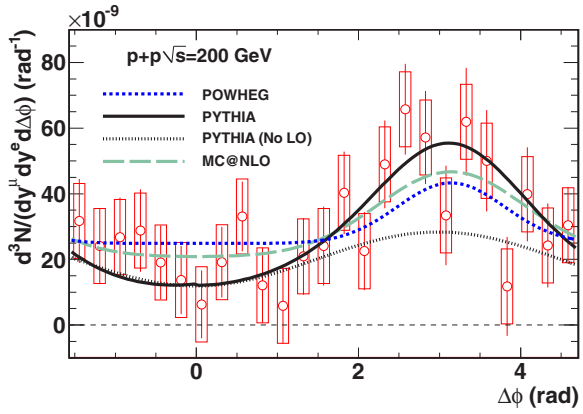

FIG. 8. (Color online) Comparison of the measured $p + p$ pair yield [(red) points] with heavy-flavor production in POWHEG ([blue] dashed curve), PYTHIA [(black) solid curve], and MC@NLO [(green) long dashed curve]. The e-μ pair yield from the subset of PYTHIA events, when the $c\bar{c}$ is not produced at the event vertex, is plotted as the dotted (black) curve. Each Monte Carlo curve was scaled by a single parameter to match the observed yield. The resulting cross sections are consistent with the previously measured charm cross sections at RHIC (see Table II).

was performed. An overall scale factor was used to fit the PYTHIA curve to the $p + p$ data. In the fit, the χ^2 was calculated for different scale parameters using the statistical error on the $p + p$ data. We report the cross section for the scale factor that minimizes that χ^2 and report a statistical error on the cross section as the value that changes the χ^2 by one unit. To evaluate the systematic uncertainty on the cross section, the $p + p$ data were increased and decreased by their combined type B and type C systematic uncertainty and the process to determine the scale factor by finding a minimum χ^2 using the statistical uncertainty in the data was repeated. We find the PYTHIA correlation is consistent with the $p + p$ data with a $c\bar{c}$ cross section of $\sigma_{c\bar{c}} = 340 \pm 29$ (stat) ± 116 (syst) μb with a χ^2/NDF of 20.5/24. This is shown as the solid curve in Fig. 8.

The other model comparisons are from NLO generators, POWHEG and MC@NLO. These programs calculate heavy-flavor cross sections and the beginning of the parton showers at NLO. They correctly model gluon fusion and flavor excitation at NLO. The underlying event and the continuation of the shower is then handled by the event generator to which it interfaces. Here MC@NLO events were interfaced to HERWIG and POWHEG events were interfaced to PYTHIA. The qualitative features of the data are present in these correlations: the continuum and the back-to-back peak. As described for the PYTHIA fit, a single scale parameter was used to calculate a χ^2 between the generated e-μ correlations and the data using the data's statistical uncertainty. The resulting best fits for POWHEG and MC@NLO are shown in Fig. 8 as the short dashed and the long dashed lines, respectively. The extracted cross sections are $\sigma_{c\bar{c}} = 511 \pm 44$ (stat) $\pm$ 198 (syst) μb with χ^2/NDF of 23.5/24 for POWHEG and $\sigma_{c\bar{c}} = 764 \pm$ 64 (stat) $\pm$ 284 (syst) μb with χ^2/NDF of 19.2/24 for MC@NLO.

We combine the cross sections from the three models and report a measured cross section of $\sigma_{c\bar{c}} = 538 \pm 46$ (stat) $\pm$ 197 (data syst) $\pm$ 174 (model syst). The central value of the cross section is the average of the three model cross sections, while the model systematic uncertainty is the standard deviation of the three model cross sections. We did not evaluate additional model uncertainties by varying the parameters for event generation. These variations would be useful in determining the parameters for a given model that best fit the data. Here, we are concerned with extracting a cross section.

This value can be compared with previous charm cross-section measurements. From the heavy-flavor electron spectra at midrapidity, PHENIX found $\sigma_{c\bar{c}} = 567 \pm 57$ (stat) $\pm$ 224 (syst) [26] and from the dielectron mass spectrum at midrapidity, PHENIX extracted $\sigma_{c\bar{c}} = 554 \pm 39$ (stat) $\pm$ 142 (data syst) $\pm$ 200 (model syst) [30]. By reconstructing D^0 and D^* mesons, STAR found $\sigma_{c\bar{c}} = 797 \pm 210$ (stat) $\pm^{+208}_{-295}$ (syst) μb [31]. An additional measurement from STAR using D^0 and $e^{\pm}$ in $d + $Au collisions [32] found $\sigma_{c\bar{c}} = 1300 \pm$ 200 (stat) $\pm$400 (syst) μb for the charm cross section. In that measurement, the electron $R_{dA} = 1.3 \pm 0.3$ (stat) ± 0.3 (syst). While this is consistent with binary scaling within the quoted uncertainties, it is also consistent with the PHENIX measurement of enhanced production of electrons at midrapidity. Within the data systematics the value of the total charm cross section extracted here is consistent with previously published RHIC results. All of these results are summarized in Table II.

Using the PYTHIA event record, it is possible to separate the $c\bar{c}$ production into an LO component, where the $gg(q\bar{q}) \rightarrow c\bar{c}$ and a component from the PYTHIA model of NLO mechanisms of flavor excitation and gluon splitting, where the $c\bar{c}$ pair is produced in the initial- or final-state shower. The "PYTHIA (No LO)" dashed curve in Fig. 8 shows the correlations from the sample of produced PYTHIA events, where the $c\bar{c}$ were not

TABLE II. Table of measured $c\bar{c}$ cross sections and from Monte Carlo generators compared to the e-μ correlations in this analysis.

Description	$\sigma_{c\bar{c}}$ (μb)
PYTHIA e-μ	340 ± 29(stat) ± 116(syst)
POWHEG e-μ	511 ± 44(stat) ± 198(syst)
MC@NLO e-μ	764 ± 64(stat) ± 284(syst)
Combined e-μ	538 ± 46(stat) ± 197(data syst) ± 174(model syst)
PHENIX single $e^{\pm}$ [26]	567 ± 57(stat) ± 224(syst)
PHENIX dilepton (e^+e^-) [30]	554 ± 39(stat) ± 142(data syst) ± 200(model syst)
STAR $D^0 + D^*$ [31]	797 ± 210(stat)$^{+208}_{-295}$(syst)
STAR $D^0 + e$ [32]	1300 ± 200(stat) ± 400(syst)

generated in the primary event vertex of PYTHIA. The back-to-back peak at $\Delta\phi = \pi$ is dominated by the LO gluon fusion process while the continuum is due to the correlations from the higher-order processes. From an accounting from PYTHIA, we find that 32% of the e-μ pair yield results from gluon fusion, consistent with the expectations from charm production [1].

Throughout the analysis it has been assumed that semileptonic $c\bar{c}$ decay is the dominant contribution to the correlations. However, $b\bar{b}$ semileptonic decays would produce a signal in both the like- and the unlike-sign pair distributions. Up to four semileptonic decays can occur where b quarks semileptonically decay to c quarks, which subsequently semileptonically decay. We have used PYTHIA and POWHEG to check these contribution from bottom. In both cases, for electrons and muons in the kinematic region that we measure, the bottom contribution is about a factor of 100 below the charm yield. This is further corroborated by the PHENIX and STAR heavy-flavor electron measurements that show that bottom becomes significant only at p_T above 3 GeV/c [29,33]. In this analysis only 3% of the sampled electrons have a p_T above 3 GeV/c, so we expect that the bottom contribution is negligible in this measurement especially compared to the background subtraction systematic uncertainties.

B. Yields in $d + \mathrm{Au}$ and comparison to $p + p$

The fully corrected like-sign-subtracted pair yield as a function of $\Delta\phi$ for electrons with $p_T^e > 0.5$ GeV/c and $|\eta^e| < 0.5$ with forward muons with $p_T^\mu > 1.0$ GeV/c and $1.4 < \eta^\mu < 2.1$ in 0%–100% $d + \mathrm{Au}$, corresponding to the total inelastic cross section, is shown in Fig. 9. A nonzero correlations strength is observed. However, unlike the $p + p$ data, there is a much less distinct back-to-back peak near $\Delta\phi$ of π. Figure 10 shows the overlay of the $p + p$ and $d + \mathrm{Au}$ pair correlations. The $p + p$ pair correlations are scaled by the $d + \mathrm{Au}$ $\langle N_{\mathrm{coll}}\rangle = 7.59 \pm 0.43$ [20]. The peak in $d + \mathrm{Au}$ is suppressed compared to $p + p$, indicating a medium modification to the yield per collision in $d + \mathrm{Au}$.

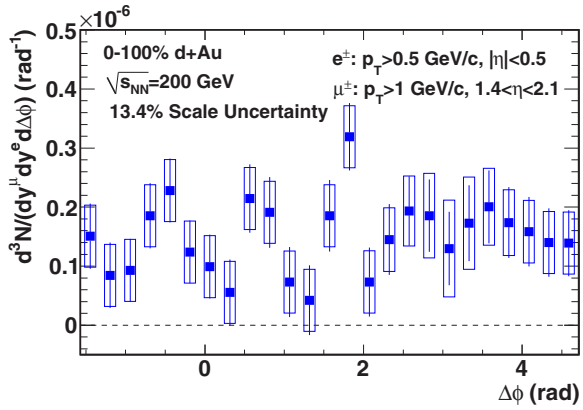

FIG. 9. (Color online) The fully corrected like-sign-subtracted heavy-flavor e-μ pair yield in $d + \mathrm{Au}$. The error bars are statistical only. The boxes show the type B systematic uncertainty from the punch-through hadron and light hadron decay muon background subtraction. The 13.4% type C systematic uncertainty is not shown.

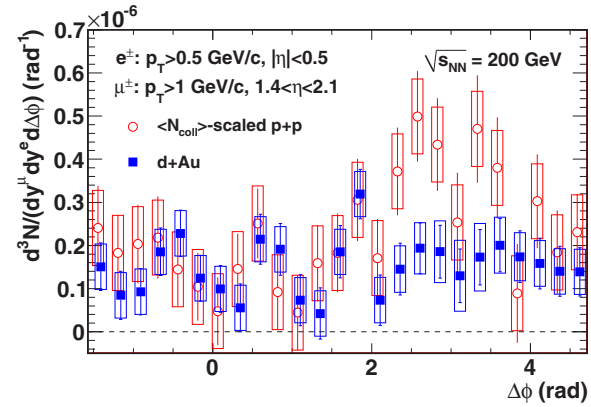

FIG. 10. (Color online) The fully corrected like-sign-subtracted heavy-flavor e-μ pair yield in [(red) circles] $\langle N_{\mathrm{coll}}\rangle$-scaled $p + p$ [(blue) boxes] $d + \mathrm{Au}$, shifted in $\Delta\phi$ for clarity. The bars are statistical uncertainty. The boxes are the type B systematic uncertainty from the decay and punch-through background subtraction. The overall normalization uncertainties of 16.1% and 13.4% in $p + p$ and $d + \mathrm{Au}$, respectively, and 5.7% uncertainty from N_{coll} are not included.

To quantify the difference between $p + p$ and $d + \mathrm{Au}$ yields, we calculate the ratio J_{dA} defined as the ratio of a pair yield in $d + \mathrm{Au}$ to the N_{coll}-scaled pair yield in $p + p$,

$$J_{dA} = \frac{d + \mathrm{Au\ pair\ yield}}{\langle N_{\mathrm{coll}}\rangle\, p + p\ \mathrm{pair\ yield}}. \tag{8}$$

Any deviation from unity of this ratio would indicate modification to the yield. When taking this ratio several systematic uncertainties common to $p + p$ and $d + \mathrm{Au}$ cancel. These are dominantly from identical cuts used in the analyses with the same systematic uncertainties. The noncancelling type C systematic uncertainties in the $p + p$ and $d + \mathrm{Au}$ yields are 7.7% and 8.9%, respectively.

Figure 11 shows a plot of J_{dA} as a function of $\Delta\phi$. The bars are statistical uncertainties and the type B systematic uncertainties are plotted as boxes. The noncancelling type C uncertainty is 14.1% and is indicated by the shaded box around one on the left. While the points near $\Delta\phi = 0$ are consistent with unity with large error bars, the points near $\Delta\phi = \pi$, where J_{dA} is about 0.4. We find

$$J_{dA}(2.7 < \Delta\phi < 3.5\,\mathrm{rad}) = 0.433 \pm 0.087\,(\mathrm{stat}) \pm 0.135\,(\mathrm{syst}) \tag{9}$$

for the bin near $\Delta\phi = \pi$. This value differs by 3.5σ from unity after combining the statistical and systematic uncertainties.

These results show that, in the measured kinematics, charm pairs are modified in the cold nuclear medium. These results are in a different kinematic region than either the single electrons, which are enhanced at midrapidity [7], or the single muons, which are suppressed at forward rapidity [10]. From the PYTHIA simulation, the e-μ correlations arise from partons in the gold nucleus with $x \approx 10^{-2}$ at $Q^2 \approx 10\,\mathrm{GeV}^2$, on the edge of the shadowing region. As discussed in Sec. IV A, the back-to-back peak is dominated by leading-order gluon fusion, while the continuum is dominated by other processes

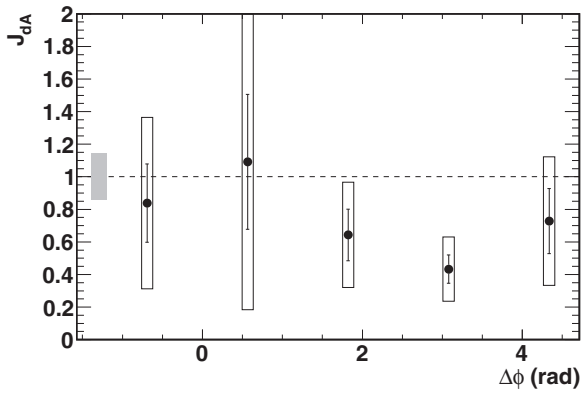

FIG. 11. J_{dA} is plotted as a function of $\Delta\phi$. The vertical bars are statistical uncertainties, the black boxes are the type B systematic uncertainties, and the gray band around 1.0 on the left is the type C systematic uncertainty. The type B systematics are symmetric around the central value but in some cases are outside the range of the plot.

like flavor excitation and gluon splitting. The observed back-to-back peak and pedestal in $p + p$ and $d + \mathrm{Au}$ should help lead to an understanding of the mechanism or mechanisms responsible for the modification. For example, the back-to-back peak is dominated by low-x gluons participating in the hard scattering, whereas the continuum has a larger contribution of quarks participating in the hard scattering. Quarks are probably less shadowed than gluons at the x and Q^2 where this analysis is measured. It is possible that there are kinematic differences between the final-state charm quarks in the peak and the continuum. These differences could affect the amount of final-state energy loss and multiple scattering that modify the measured pair yields. It may be possible to combine these results with other cold nuclear matter modifications to single-particle and pair yields in different kinematic regions to disentangle the effects of shadowing, saturation, and energy loss.

V. SUMMARY AND CONCLUSIONS

We presented PHENIX results for heavy-flavor production of azimuthally correlated unlike-sign e-μ pairs in $p + p$ and $d + \mathrm{Au}$ collisions at $\sqrt{s_{NN}}$ of 200 GeV. The $p + p$ yield shows a nonzero continuum as well as a back-to-back peak structure centered at $\Delta\phi = \pi$. When compared with several models, we find the charm cross section $\sigma_{c\bar{c}} = 538 \pm 46\ (\mathrm{stat}) \pm 197\ (\mathrm{data\ syst}) \pm 174\ (\mathrm{model\ syst})\ \mu\mathrm{b}$. This is also consistent with previously measured $c\bar{c}$ cross sections at this center of mass energy. In $d + \mathrm{Au}$ collisions a yield reduction in the back-to-back peak is observed, where we measure $J_{dA}(2.7 < \Delta\phi < 3.5\,\mathrm{rad}) = 0.433 \pm 0.087\ (\mathrm{stat}) \pm 0.135\ (\mathrm{syst})$. This indicates that the nuclear medium modifies the $c\bar{c}$ correlations in the measured p_T and rapidity windows of this analysis. Such a suppression could arise due to nuclear PDF shadowing, saturation of the gluon wave function in the Au nucleus or initial- or final-state energy loss and multiple scattering.

ACKNOWLEDGMENTS

We thank the staff of the Collider-Accelerator and Physics Departments at Brookhaven National Laboratory and the staff of the other PHENIX participating institutions for their vital contributions. We acknowledge support from the Office of Nuclear Physics in the Office of Science of the Department of Energy, the National Science Foundation, a sponsored research grant from Renaissance Technologies LLC, Abilene Christian University Research Council; Research Foundation of SUNY, and Dean of the College of Arts and Sciences, Vanderbilt University (U.S.A.); Ministry of Education, Culture, Sports, Science, and Technology and the Japan Society for the Promotion of Science (Japan); Conselho Nacional de Desenvolvimento Científico e Tecnológico and Fundação de Amparo à Pesquisa do Estado de São Paulo (Brazil); Natural Science Foundation of China (P. R. China); Ministry of Education, Youth and Sports (Czech Republic); Centre National de la Recherche Scientifique, Commissariat à l'Énergie Atomique, and Institut National de Physique Nucléaire et de Physique des Particules (France); Bundesministerium für Bildung und Forschung, Deutscher Akademischer Austausch Dienst, and Alexander von Humboldt Stiftung (Germany); Hungarian National Science Fund, OTKA (Hungary); Department of Atomic Energy and Department of Science and Technology (India); Israel Science Foundation (Israel); National Research Foundation and WCU program of the Ministry Education Science and Technology (Korea); Physics Department, Lahore University of Management Sciences (Pakistan); Ministry of Education and Science, Russian Academy of Sciences, Federal Agency of Atomic Energy (Russia); VR and Wallenberg Foundation (Sweden); the U.S. Civilian Research and Development Foundation for the Independent States of the Former Soviet Union; the US-Hungarian Fulbright Foundation for Educational Exchange; and the US-Israel Binational Science Foundation.

[1] N. Brambilla *et al.*, Eur. Phys. J. C **71**, 1534 (2011).
[2] F. Gelis, E. Iancu, J. Jalilian-Marian, and R. Venugopalan, Annu. Rev. Nucl. Part. Sci. **60**, 463 (2010).
[3] X.-N. Wang and X.-F. Guo, Nucl. Phys. A **696**, 788 (2001).
[4] L. Frankfurt and M. Strikman, Phys. Lett. B **645**, 412 (2007).
[5] I. Vitev, Phys. Rev. C **75**, 064906 (2007).
[6] A. M. Sickles, Phys. Lett. B **731**, 51 (2014).
[7] A. Adare *et al.* (PHENIX Collaboration), Phys. Rev. Lett. **109**, 242301 (2012).
[8] A. Adare *et al.* (PHENIX Collaboration), Phys. Rev. C **87**, 034904 (2013).
[9] L. Adamczyk *et al.* (STAR Collaboration), arXiv:1312.3675.
[10] A. Adare *et al.* (PHENIX Collaboration), arXiv:1310.1005.
[11] A. Adare *et al.* (PHENIX Collaboration), Phys. Rev. Lett. **107**, 172301 (2011).
[12] E. Braidot, Ph.D. thesis, Utrecht University, 2011.
[13] Z.-B. Kang, I. Vitev, and H. Xing, Phys. Rev. D **85**, 054024 (2012).
[14] A. Stasto, B.-W. Xiao, and F. Yuan, Phys. Lett. B **716**, 430 (2012).
[15] J. Jalilian-Marian and A. H. Rezaeian, Phys. Rev. D **86**, 034016 (2012).

[16] T. Lappi and H. Mäntysaari, Nucl. Phys. A **908**, 51 (2013).
[17] K. Adcox *et al.* (PHENIX Collaboration), Nucl. Instrum. Methods A **499**, 469 (2003).
[18] T. Sjöstrand, S. Mrenna, and P. Skands, J. High Energy Phys. **05**, 026 (2006).
[19] L. Aphecetche *et al.* (PHENIX Collaboration), Nucl. Instrum. Methods A **499**, 521 (2003).
[20] A. Adare *et al.* (PHENIX Collaboration), arXiv:1310.4793.
[21] S. S. Adler *et al.* (PHENIX Collaboration), Phys. Rev. D **76**, 092002 (2007).
[22] A. Adare *et al.* (PHENIX Collaboration), Phys. Rev. C **84**, 044905 (2011).
[23] S. S. Adler *et al.* (PHENIX Collaboration), Phys. Rev. C **73**, 054903 (2006).
[24] D. Hornback, Ph.D. thesis, University of Tennessee, 2007.
[25] W. Vogelsang (private communication).
[26] A. Adare *et al.* (PHENIX Collaboration), Phys. Rev. Lett. **97**, 252002 (2006).
[27] S. Frixione, G. Ridolfi, and P. Nason, J. High Energy Phys. **09**, 126 (2007).
[28] S. Frixione and B. R. Webber, J. High Energy Phys. **06**, 029 (2002).
[29] A. Adare *et al.* (PHENIX Collaboration), Phys. Rev. Lett. **103**, 082002 (2009).
[30] A. Adare *et al.* (PHENIX Collaboration), Phys. Rev. D **79**, 012003 (2009).
[31] L. Adamczyk *et al.* (STAR Collaboration), Phys. Rev. D **86**, 072013 (2012).
[32] J. Adams *et al.* (STAR Collaboration), Phys. Rev. Lett. **94**, 062301 (2005).
[33] M. M. Aggarwal *et al.* (STAR Collaboration), Phys. Rev. Lett. **105**, 202301 (2010).